# Chemical and Electronic Effects of Ni in Pt/Ni and Pt/Ru/Ni Alloy Nanoparticles in Methanol Electrooxidation

**Kyung-Won Park, Jong-Ho Choi, Boo-Kil Kwon, Seol-Ah Lee, and Yung-Eun Sung***

*Department of Materials Science & Engineering, Kwangju Institute of Science & Technology, Kwangju 500-712, South Korea*

**Heung-Yong Ha and Seong-Ahn Hong**

*Battery & Fuel Cell Research Center, Korea Institute of Science & Technology, Seoul 136-791, South Korea*

**Hongsun Kim and Andrzej Wieckowski***

*Department of Chemistry & Fredrick Seitz Materials Research Laboratory, University of Illinois at Urbana−Champaign, Urbana, Illinois 61801*

*Received: August 17, 2001; In Final Form: December 17, 2001*

Electrooxidation of methanol in sulfuric acid solution was studied using Pt, Pt/Ni(1:1 and 3:1), Pt/Ru/Ni(5:4:1 and 6:3.5:0.5), and Pt/Ru(1:1) alloy nanoparticle catalysts, in relation to methanol oxidation processes in the direct oxidation methanol fuel cell. The Pt/Ni and Pt/Ru/Ni alloys showed excellent catalytic activities compared to those of pure Pt and Pt/Ru. The role of Ni as a catalytically enhancing agent in the oxidation process was interrogated using cyclic voltammetry, chronoamperometry, X-ray photoelectron spectroscopy, transmission electron microscopy, and X-ray diffraction. X-ray diffraction data showed alloy formation for all Pt/Ni, Pt/Ru/Ni, and Pt/Ru nanoparticles, whereas X-ray photoelectron spectroscopy confirmed that chemical states of Pt were exclusively metallic. The presence of metallic Ni, NiO, $Ni(OH)_2$, NiOOH, metallic Ru, $RuO_2$, and $RuO_3$ was also confirmed. We found that the Pt*4f* binding energies for the Pt/Ni and Pt/Ru/Ni alloy nanoparticles were lower than those for clean Pt nanoparticles. The oxides that serve as the oxygen donors for the oxidation process, and the change in the electronic structure of the Pt component in the alloys versus those in Pt and Pt/Ru collectively account, we believe, for enhancement in rates of methanol oxidation. The difference in the peak shift in Pt*4f* between Pt/Ni and Pt/Ru alloy nanoparticles is discussed by using electronegativities of the three components: Pt, Ru, and Ni. A comparison between the alloy nanoparticle composition and that of disk alloy electrodes under similar conditions was made in terms of the surface-to-volume ratio and surface segregation of the alloying components.

## Introduction

The direct oxidation methanol fuel cell (DMFC), which uses methanol directly as fuel, has been a subject of intense study because of numerous advantages of the DMFC, such as high energy density, ease of handling a liquid, and low operating temperatures.[1−6] High activity of methanol oxidation on platinum makes this metal a suitable electrocatalyst for the DMFC anode. However, as well-known, pure platinum at room or moderate temperatures is readily poisoned by carbon monoxide (CO), a byproduct of methanol oxidation. To date, the remedy has been to use alloy or ternary catalysts based upon platinum, all contain ruthenium as the activity promoting component.[7−16] According to the bifunctional mechanism, the CO poisoned platinum is regenerated via reaction of surface CO with O-type species associated with ruthenium to yield $CO_2$.[14,15] Beyond the applicability range of this mechanism, Goodenough et al. reported a shift in the Pt*4f* peak of a Pt/Ru alloy using X-ray photoelectron spectroscopy (XPS) analysis,[17] showing that some electronic effects (ligand effects) can also be involved in the ruthenium enhancement.[3,6,10,14−16] Also, the change in the electronic properties of Pt/Ni, Pt/Co, and Pt/Fe disks have been identified by a d-vacancy shift of XPS,[18] and single-crystal studies have provided important new insights into surface structural effects involved in the Pt/Ru catalysis.[6,19−25] Overall, the issue of whether the second metal is involved in the modification of the Pt electronic structure is unclear. Previous studies have not taken into account, for instance, the combination of chemical states, electronic structure, and geometric factors in constructing a global picture of the electrocatalysis on multicomponent alloy surfaces. Therefore, further progress in fuel cell catalysis, especially on a nanoparticle surface, and the catalyst optimization are needed. Syntheses of such new, more potent catalysts should be directed toward higher surface-to-volume ratios of catalyst particles; reduction of the amount of precious metal loadings; increasing the desired electronic, geometric, and structural modification; and a particle size control.[26]

Our previous work involving the use of arc-melted Pt/Ru and Pt/Os alloy electrodes provided an evidence that the surface segregation (i.e., Pt enrichment on the surface) occurred and that the alloy surface composition varied with the electrode potential.[16] Most researchers, however, agree that structural factors involved in catalysis by small particles differ from those at smooth electrodes.[27−29] The use of nanoparticles may change

* To whom correspondence should be addressed.

10.1021/jp013168v CCC: $22.00 
Published on Web 02/02/2002

the nature of phase diagrams and segregation at the alloy surface from bulk material due to their different number of layers related to surface, subsurface, and bulk compositions.[30] A considerable controversy exists, for instance, whether the particle size is important. Watanabe et al.[31] were unable to find any evidence for such an effect in methanol oxidation, but some other studies have confirmed the need for the particle size optimization.[32,33] Recently, measurements with Pt/Ru catalysts have been conducted via X-ray absorption spectroscopy[5,34] and by electrochemical nuclear magnetic resonance[35−37] in order to elucidate these issues.

For the Pt/Ni nanoparticles of interest to this project, model calculations by Abraham et al. predicted that the segregation processes of the type mentioned above should not be occurring.[38,39] Some form of surface enrichment must, however, take place. For instance, it was found that heating catalysts in air led to better results than heating in the presence of hydrogen because of surface enrichment in Pt.[40] Another issue is the occurrence of intermetallic charge transfer in the relevant alloy systems. Because of the electron transfer from Ru to Pt within the Pt/Ru alloys for instance[17] and the reduction in local density of states (DOS) on the Fermi level, the electron density on the $2\pi^*$ molecular orbital of adsorbed CO is reduced, as demonstrated recently.[41] On the similar line, Goodman et al. discussed relevant correlations between CO chemisorption energy and the surface core level shifts in XPS.[42−44]

Because the bonding energy of Ru−O is similar to that of Pt−C,[45−47] Ru in the Pt/Ru easily oxidizes the CO intermediate to $CO_2$ by the bifunctional mechanism (see above). However, because the energy of the Ni−O bond is by ∼200 kJ/mol lower than that of Pt−C, some essential characteristics of Pt/Ni must not be explained by the bifunctional mechanism alone. Also, data on the electronic effects involved in alloying platinum with transition metals other than ruthenium are rare.[48−51] Therefore, in this paper, electrocatalytic properties of Pt/Ni and Pt/Ru/Ni alloy nanoparticles were investigated. To decipher the oxidation mechanism and the reasons for the enhancement of activity toward methanol oxidation, various analyses such as X-ray diffraction (XRD), XPS, transmission electron microscopy (TEM), and electrochemical measurements were performed. The surface oxidation states of the individual components of the alloy particles were obtained by XPS, and were correlated to XRD and electrochemical data. Such data provide, we believe, a comprehensive insight into DMFC electrooxidation mechanisms on the Pt/Ni and Pt/Ru/Ni surfaces.

## Experimental Section

Pt-based catalysts were synthesized at room temperature using a conventional reduction method with $NaBH_4$.[52,53] Pt salt ($H_2PtCl_6 \cdot xH_2O$, Aldrich Chem. Co.), Ni salt ($NiCl_2 \cdot 6H_2O$, Aldrich Chem. Co.), and Ru salt ($RuCl_3 \cdot xH_2O$, Aldrich Chem. Co.) were mixed in Millipore water (18 MΩ cm) until dissolved completely. After several hours, the salts were reduced with $NaBH_4$ (Aldrich Chem. Co.) under constant stirring. The amount of the $NaBH_4$ reducing agent was over 1.5 times that of the valencies of the transition metal cations, which was sufficient to reduce the metal salts to the elemental state. The resulting material was washed with deionized water and dried by freeze-drying.

X-ray diffraction (XRD) analyses of Pt-based catalysts were carried out using an in-house fabricated X-ray powder diffractometer equipped with a Cu Kα (8.05 keV) source. To estimate the size and composition of the platinum alloy particles, the (220) peak was fitted using the Lorentzian/Gaussian function. The size and composition were obtained by the use of the Debye−Scherrer equation and the Vegard's law (see the Results and Discussion section). The size of metal particles was investigated by transmission electron microscopy (TEM) on a JEOL instrument (JEM-2000FXII) at 200 kV accelerating potential. Specimens were prepared by ultrasonically suspending the particles in deionized water. Drops of such suspensions were deposited onto a standard Cu grid covered with carbon film (200 mesh) and allowed to dry before being inserted into the microscope. The EDX analysis was performed at 200 kV using an EXL II, Oxford attached to the microscope.

XPS analyses were performed using a PHI 5400 model of the 5400 X-ray Physical Electronics photoelectron spectrometer. The X-ray source was Mg Kα with 1253.6 eV operating at 15 kV and 500 W. Samples were prepared by depositing the catalyst on a Cu double-sided tape (3M Inc.). The base pressure of the system was $10^{-10}$ Torr. The XPS core-level spectra were fitted to the Doniach−Sunjic line shape convoluted by a Gaussian contribution taking into account the spectrometer resolution. Background removal was carried out using the Shirley baseline method.[54] Both ends of the baseline were set sufficiently far so as not to distort the shape of spectra, including tails. Small variation of the range of the baseline did not affect the relative amount of fitted species (less than 1%). As we reported previously, all binding energies were calibrated by referencing Au$4f_{7/2}$ (84.0 eV) and Cu$2p_{3/2}$ (932.66 eV) of sputter-cleaned Au and Cu.[16] For homogeneous alloys of AB or ABC, a simple linear expression furnishes quantitative results.[55,56] We either experimentally measured the pure element intensities (e.g., pure Pt and a thick layer of Ru on Pt) or used sensitivity factors for Pt*4f*, Ru*3d*, and Ni*2p* from the literature.[16,57,58] This simple relationship permits estimations of the number of monolayers but not the surface coverage. The surface coverage on the alloys was determined by XPS using a modified relative ratio method.[16]

Electrochemical measurements were made using a three-electrode cell at 25 °C. A Pt wire and an Ag/AgCl (in saturated KCl) were used as the counter and reference electrodes, respectively. All potentials are reported vs NHE in this paper. The carbon electrode as working electrode was polished with 1, 0.3, and 0.05 μm $Al_2O_3$ paste and washed ultrasonically in a Millipore water (18 MΩ cm). The working electrode was brushed with the catalyst ink as described previously.[59] Solutions of 0.5 M $H_2SO_4$ and 2.0 M $CH_3OH$ in 0.5 M $H_2SO_4$ were stirred constantly and purged with nitrogen gas. All chemicals used were of analytical grade. Electrochemical experiments were performed with AUTOLAB by Eco Chemie. To identify the properties of the Pt-based catalyst in $H_2SO_4$ and to measure the onset potential of methanol oxidation, cyclic voltammetry (CV) was performed in the potential between −0.08 and 1.52 V vs NHE. Chronoamperometric (CA) curves of 2.0 M $CH_3OH$ + 0.5 M $H_2SO_4$ were measured for 1 h maintaining a potential of 0.42 V vs NHE reference.

## Results and Discussion

**XRD, TEM, and EDX Analysis of Pt/Ni, Pt/Ru, and Pt/Ru/Ni Nanoparticles.** XRD analyses clearly demonstrate the characteristic peaks of the Pt fcc structure. In Figure 1a, no peaks for fcc Ni and hcp Ru metals or oxides/hydroxides are shown. The $2\theta$ of the (111) peak for Pt/Ni(1:1), Pt/Ni(3:1), Pt/Ru(1:1), and Pt/Ru/Ni(5:4:1), which have angle shifts higher than 39.83 of pure Pt, are 41.59, 40.13, 40.28, and 40.37, respectively, as seen in Figure 1b. Same trend was also shown in $2\theta$ of the (220) peaks [67.71 (Pt), 70.11 (Pt/Ni(1:1)), 68.31 (Pt/Ni(3:1)), 68.46 (Pt/Ru(1:1)), 68.64 (Pt/Ru/Ni(5:4:1))]. The higher angle shifts of the Pt peaks account for the alloy formation between

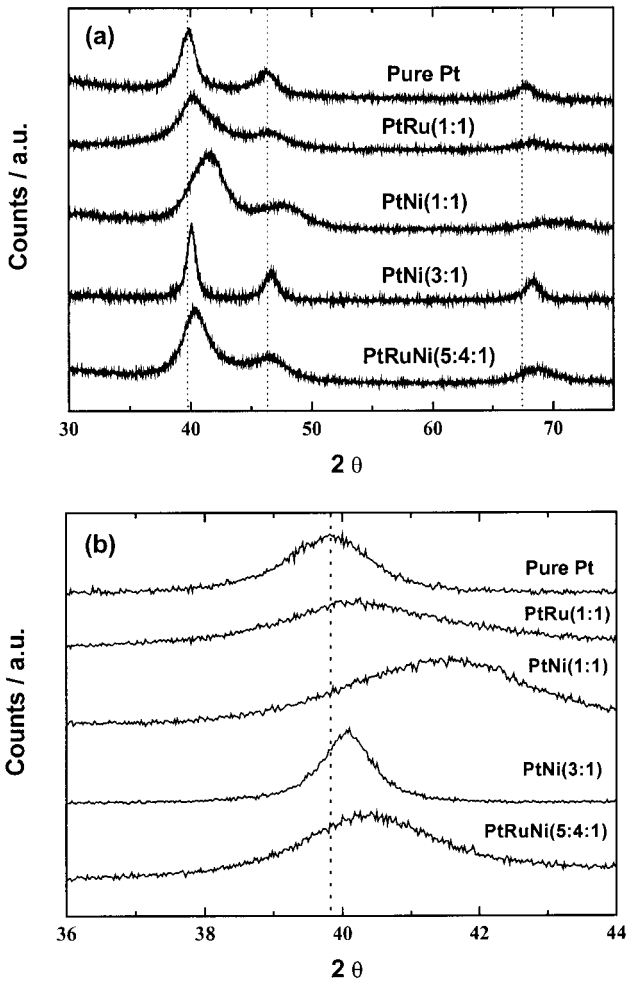


**Figure 1.** X-ray diffraction analysis of Pt based nanoparticles; (a) wide scanning of X-ray diffraction and (b) fine scanning of (111) peak.

Pt and Ni, and Ru. Pt/Ru(1:1) is known to alloy well.[47,48] In the present data, Pt/Ni(1:1) has higher peak shift than Pt/Ru(1:1), suggesting a good alloy formation. The trends for Pt/Ni(3:1) and Pt/Ru/Ni(5:4:1) are between them, depending on the amounts of the second and third metals. By fitting the (220) peak, it is clear that the *d* spacing of (220) in the Pt/Ni(1:1), PtNi(3:1), Pt/Ru(1:1), and Pt/Ru/Ni(5:4:1) alloy nanoparticles are 1.3406, 1.3715, 1.3688, and 1.3657, whereas those of pure Pt and Ni are 1.387 and 1.240. Pt/Ni alloys have most likely a metallic nickel in the platinum lattice, and the metallic grains are intermixed with amorphous Ni oxides, such as NiO, Ni-$(OH)_2$, and NiOOH (see XPS data below). Another possibility is that the oxides are present at the grain surfaces. Possible segregation of Pt to the surface may not be detected in XRD since the X-ray energy is sufficiently high to transmit to the size range of nanoparticles.

After subtraction of contributions from Cu K$\alpha_2$ the (220) peak was fitted with a mixed Gaussian−Lorentzian line shape, according to Radmilovic et al.[60] In the XRD peak analysis the average size of a particle is about 3−4 nm, as calculated using the Debye−Scherrer (eq 1), where the $L$ is average particle size, $\lambda_{K\alpha1}$ is the wavelength of X-ray, $\theta_B$ is the angle of (220) peak, and $B_{(2\theta)}$ is the peak broadening.

$$L = \frac{0.94\lambda_{K\alpha1}}{B_{(2\theta)}\cos\theta_B} \quad (1)$$

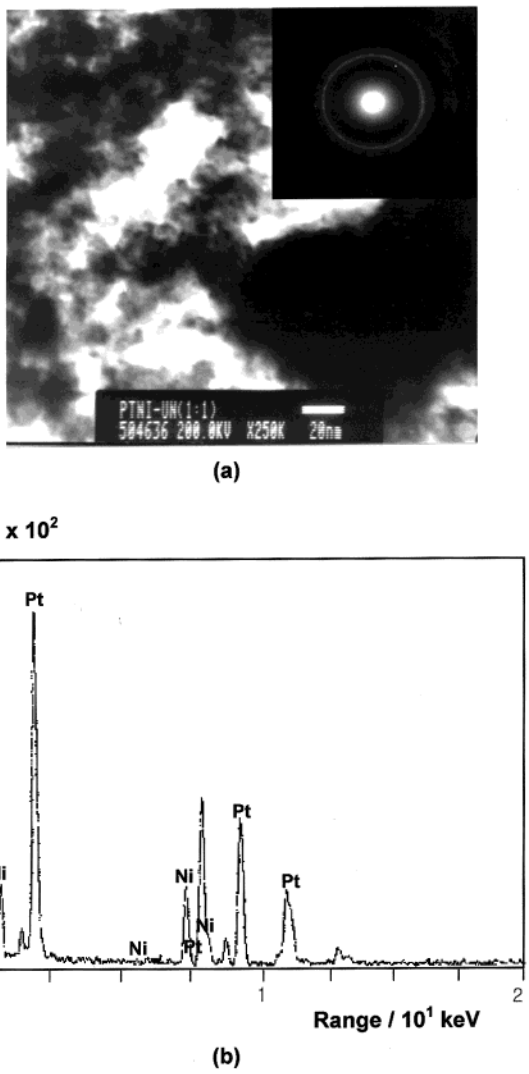


**Figure 2.** Bright field image of Pt/Ni(1:1) nanoparticle by (a) transmission electron microscopy, (insert) transmission electron diffraction pattern, and (b) EDX spectrum.

The size of the alloy nanoparticles was also investigated by TEM. In Figure 2a for the unsupported Pt/Ni(1:1) example, the particle size is approximately 3−4 nm, which is in good agreement with the XRD data. Unlike the unsupported samples, the nanoparticle on carbon support showed a homogeneous dispersion with a similar particle size. The particle was largely spherical in shape. The circular shape of the patterns in Figure 2 (insert) indicates that these nanosized particles are formed from the crystalline powder. No agglomerations were observed with unsupported particles. EDX analysis was again carried out in order to obtain information on the chemical properties of the nanoparticles. In Figure 2b, the EDX spectra of the Pt/Ni-(1:1) nanoparticles indicate a 1:1 atomic ratio of the particle in various portions of the nanoparticle powders. Therefore, the borohydride reduction method combined with the freeze-drying procedure resulted in producing small particle, highly dispersed Pt/Ru, Pt/Ni, and Pt/Ru/Ni catalysts as compared to those obtained by typical borohydride reduction method.[52,53]

**Voltammetry and Chronoamperometry.** The Pt alloy nanoparticles were analyzed in 0.5 M $H_2SO_4$ and 2.0 M $CH_3$-OH/0.5 M $H_2SO_4$ solution using voltammetry. Cyclic voltammograms (CV) of the nanoparticles in 0.5 M $H_2SO_4$ at room temperature were obtained during scanning between 0.0 and 1.6 V vs NHE with a scan rate of 50 mV $s^{-1}$. The CV of Pt/

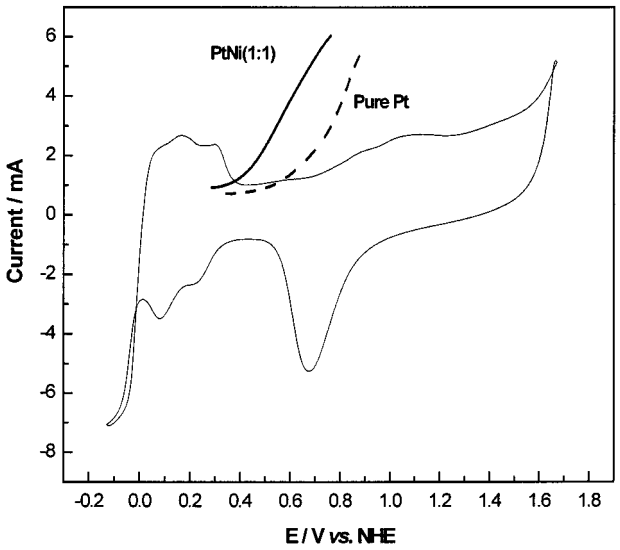


**Figure 3.** Potential−current plots for Pt/Ni(1:1) in 0.5 M $H_2SO_4$, and Pt/Ni(1:1) and Pt for methanol oxidation in 2.0 M $CH_3OH$ + 0.5 M $H_2SO_4$ with the scan rate of 50 mV $s^{-1}$ at room temperature.

**TABLE 1: Onset Potentials for Methanol Oxidation Using Pt-Based Alloy Nanoparticles in 2.0 M $CH_3OH$ + 0.5 M $H_2SO_4$**

| Pt alloys | onset potential (vs NHE) |
|---|---|
| pure Pt | 0.350 |
| Pt/Ru (1:1) | 0.265 |
| Pt/Ni (1:1) | 0.290 |
| Pt/Ni (3:1) | 0.320 |
| Pt/Ru/Ni (5:4:1) | 0.261 |
| Pt/Ru/Ni (6:3.5:0.5) | 0.287 |

Ni(1:1) nanoparticle electrode indicates the presence of polycrystalline Pt in Figure 3 (thin solid line). The peaks for the adsorption/desorption of hydrogen and preoxidation/reduction on the Pt surface in $H_2SO_4$ are clearly shown. No characteristic features of Ni oxidation were found. In contrast, the Pt/Ru and Pt/Ru/Ni ternary nanoparticle electrodes have a very thick double layer because of the RuOH and higher oxides presence in the surface layer.

Methanol oxidation current measured on the Pt/Ni based catalysts in 2.0 M $CH_3OH$ + 0.5 M $H_2SO_4$ at room temperature (at 50 mV $s^{-1}$) exceeds that obtained with pure Pt. The comparison of the onset potentials for methanol oxidation on Pt/Ni(1:1) (thick solid line) and on Pt (dotted line) in Figure 3 indicates that the Pt/Ni nanoparticles show relatively good electrocatalytic activity (Table 1). Theoretically, methanol oxidation may proceed at 0.04 V vs NHE.

$$CH_3OH + H_2O \rightarrow CO_2 + 6H^+ + 6e^- \qquad (2)$$

Therefore, the lower onset potential indicates clear evidence for superior electrocatalytic activity for methanol electrooxidation. In Table 1, most of the binary and ternary catalysts have lower onset potentials and a higher current than pure Pt, and Pt/Ru/Ni(5:4:1) shows the lowest onset potential. Pt/Ni(1:1) and Pt/Ru/Ni(6:3.5:0.5) electrocatalysts have fairly good electrocatalytic activity toward methanol oxidation compared with Pt/Ru(1:1). The onset potential of Pt/Ni(3:1) is rather higher than that for other Pt/Ni based catalysts and is similar to that of pure Pt.

Using Pt alloy nanoparticles, plots of oxidation current vs time (chronoamperometry, CA) were measured in 2.0 M $CH_3OH$ + 0.5 M $H_2SO_4$ at 0.42 V, for 3600 s. Figure 4 shows such typical $i-t$ plots with the current normalized to the initial current ($i_{meas}/i_o$). For each catalyst, the decay in the methanol oxidation is different; for instance, pure platinum nanoparticles require 10 min to reach 70% of the initial current and the oxidation current is reduced steeply. After 1 h, the current decreases below 40% of the initial value. In contrast, Pt/Ni(1:1), Pt/Ru(1:1), and Pt/Ru/Ni(5:4:1) support higher current, and one may conclude that they have higher activity than pure Pt. From the comparative data, one may also conclude that Pt/Ru(1:1) is the most active surface, which is followed by Pt/Ni(1:1). However, after ca. 15 min, Pt/Ru/Ni(5:4:1) supports quite high oxidation current as compared to Pt/Ru(1:1) and Pt/Ni(1:1). The Pt/Ru/Ni(5:4:1) needs 1 h to reach 74% of the initial current, whereas Pt/Ru(1:1) reaches the same current ratio after half hour. The current measured at 1 h at Pt/Ru/Ni (5:4:1) is 2 orders of magnitude higher than that obtained with pure Pt. The current is also about 1 order of magnitude higher than for Pt/Ru(1:1). The order of surface activity for the methanol oxidation is therefore Pt/Ru/Ni(5:4:1) > Pt/Ni(1:1) > Pt/Ru(1:1) > Pt. By combing voltammetry and CA, we can conclude that Pt/Ru/Ni(5:4:1) and Pt/Ni(1:1) represent the best alternative candidates for the DMFC anode catalysts with respect to Pt/Ru.

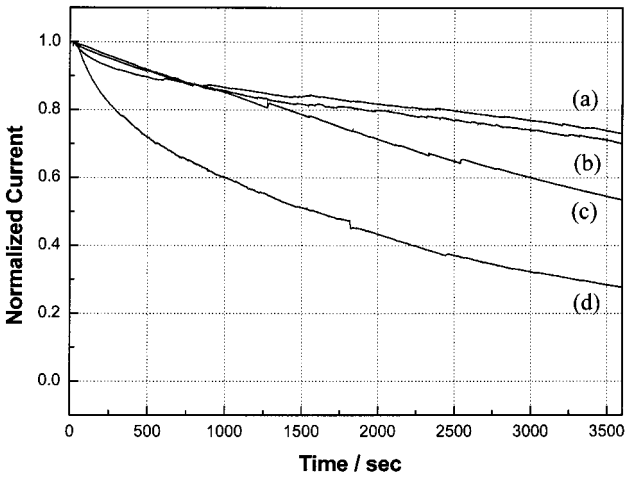


**Figure 4.** Current−time plots of (a) Pt/Ru/Ni(5:4:1), (b) Pt/Ni(1:1), (c) Pt/Ru(1:1), and (d) pure Pt in 2.0 M $CH_3OH$ + 0.5 M $H_2SO_4$ with a constant potential of 0.42 V vs NHE at room temperature.

**X-ray Photoelectron Spectroscopy.** No XPS peaks for chloride were found showing that the metal salts were completely removed during washing. For Pt/Ni(1:1), Pt/Ni(3:1), Pt/Ru/Ni(5:4:1), and Pt/Ru(1:1) alloy nanoparticles, Pt*4f* spectra are shown in Figures 5a−8a. The Pt$4f_{7/2}$ and $4f_{5/2}$ lines appear at ∼71 and ∼74 eV, respectively, with the theoretical ratio of peak areas of 4:3. The comparison of the binding energies indicates that Pt is present in the zerovalent metallic state in all alloy nanoparticles. That is, the peaks for $Pt^{2+}$ and $Pt^{4+}$ at 73.8 and 74.6 eV, respectively, were not found. When the XPS data is compared using the monochromatic Al Kα line, no evidence for the photoreduction of platinum oxides was found.[16] In the Pt/Ni alloy nanoparticles, the Ni states shown in Figures 5−7 consist of Ni metal ($Ni^o$) as well as Ni oxide and hydroxides (NiO, $Ni(OH)_2$, and NiOOH). In general, the Ni$2p_{3/2}$ spectrum shows a complex structure with an intense satellite signals of high binding energy adjacent to the main peaks, which can be attributed to multielectron excitation.[61−70] After these shake-up peaks are considered, the Ni$2p_{3/2}$ XPS peaks at the binding energies of 852.7, 853.8, 855.6, and 857.3 eV correspond to $Ni^o$, NiO, $Ni(OH)_2$, and NiOOH, respectively.[61−72] The Ni*2p*

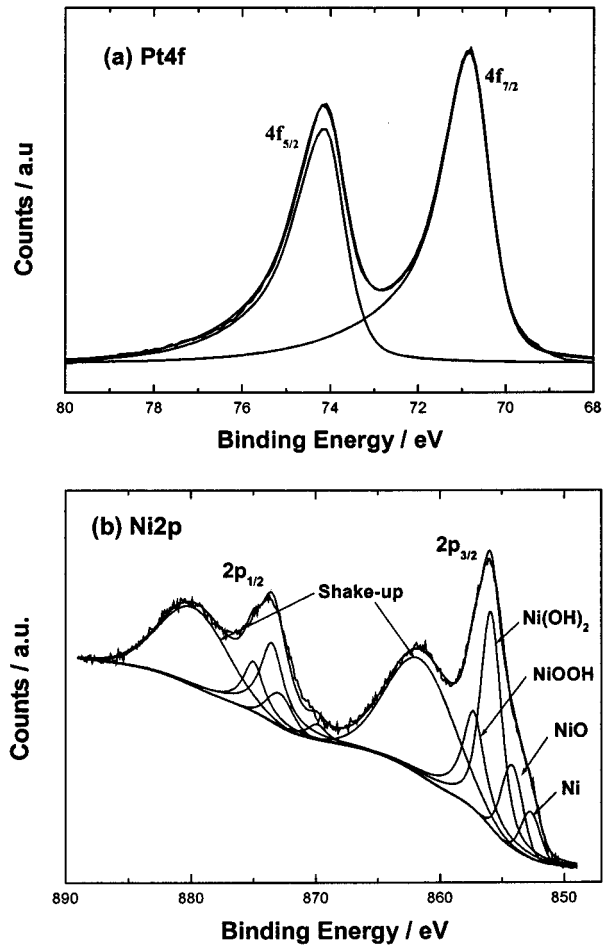


**Figure 5.** X-ray photoelectron spectra of (a) Pt*4f* and (b) Ni*2p* in Pt/Ni(1:1) nanoparticle.

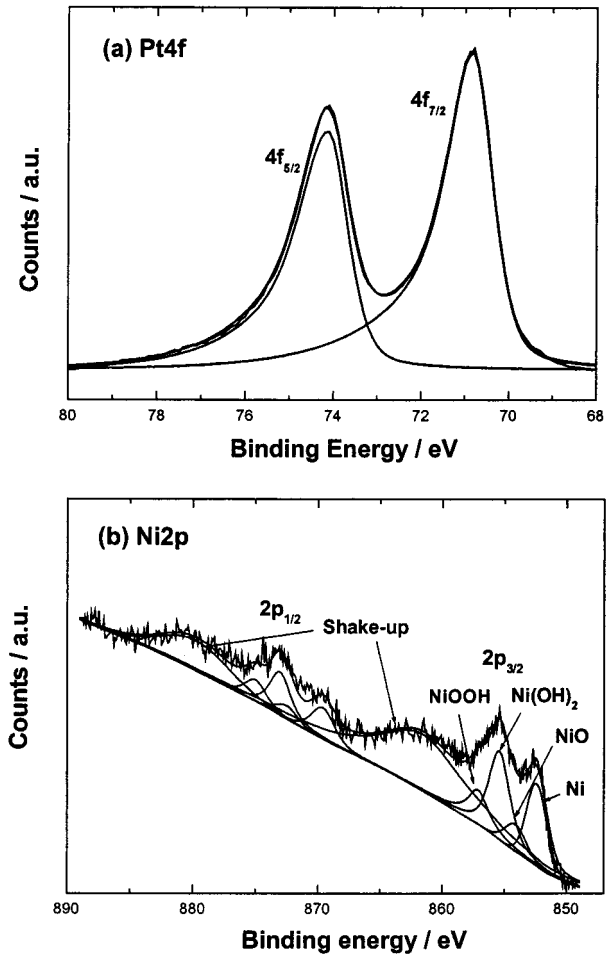


**Figure 6.** X-ray photoelectron spectra of (a) Pt*4f* and (b) Ni*2p* in Pt/Ni(3:1) nanoparticle.

spectra (Figure 7b) of the Pt/Ru/Ni ternary catalyst has $Ni^o$, NiO, $Ni(OH)_2$, and NiOOH, as also seen in the Pt/Ni nanoparticles. The Ru*3d* spectra (Figure 7c) of the Pt/Ru/Ni consist of the chemical states, $Ru^0$, $RuO_2$, and $RuO_3$, as those of Pt/Ru-(1:1) in Figure 8b and of the disk Pt/Ru electrodes.[16] The Ru*3d* region of the Pt alloy XPS spectra is often obscured by the strong C*1s* signal because of surface contamination by carbon. However, our XPS had a sufficient signal-to-noise ratio in the Ru*3d* region to resolve ruthenium from any C contamination C signal, permitting assignments of the Ru peaks after peak fittings. Metallic ruthenium appears as a spin−orbit doublet at 279.9 ($Ru3d_{5/2}$) and 284.1 eV ($Ru3d_{3/2}$) with the area ratio of 1.5. $RuO_2$ was characterized using $3d_{5/2}$ and $3d_{3/2}$ peaks located at 281.2 and 285.4 eV, respectively. Additional Ru peaks were found at 282.7 and 286.9 eV, indicating a formation of the second Ru oxide, $RuO_3$. These findings indicate that the surface of Pt/Ru/Ni may display combined catalytic properties of Pt/Ni and Pt/Ru.

According to the bifunctional mechanism, oxophilic Ru sites covered by RuOH are the source of oxygen needed for surface CO removal, and as a result, Pt/Ru has excellent catalytic activity compared to pure Pt. The major component of Pt/Ni is nickel hydroxide, $Ni(OH)_2$, Table 2. At Pt/Ni(1:1), the Ni additive is comprised of 11.8% metallic Ni, 15.9% NiO, 45.2% $Ni(OH)_2$, and 27.1% NiOOH. The Pt/Ni(3:1) nanoparticle has 33.7% metallic Ni and a decreased level of Ni oxides. For Pt/Ru/Ni(5:4:1), the makeup is 14.4% metallic Ni and 11.2% NiO. However, the ratios between the three oxides are similar. The issue of whether metallic Ni exists on the surface, on the basis of this XPS study, is unclear. The enhanced activity of the Pt/Ni alloy may be related to the modification of the electronic structure of platinum in the nanoparticles by electron transfer from Ni to Pt, see below.[14,15]

It is important to know the composition of the surface in order to evaluate some possible electronic effects in the catalytic properties of the alloy. The Pt/Ni and Pt/Ru/Ni nanoparticles employed herein showed enrichment of Pt at the surface relative to the bulk. For instance, Pt/Ni(1:1) had 53.4 atomic % of Pt vs 46.6% Ni. It is known that, given a similar size, the metal having the lower heat of sublimation tends to surface segregate in binary alloys. The heats of vaporization of Pt, Ni, and Ru are 509.6, 370.3, and 589.9 kJ/mol, respectively.[73] Therefore, Ni should be enriched in the surface from this explanation. However, strong surface enrichment in Pt was found by low-energy ion scattering (LEIS) in Pt/Ni alloys.[37,38] This demonstrates that the thermodynamic explanation fails to predict the enrichment behaviors. Further, Mukerjee et al.[74] used the electronic theory of d-band density of states of pure components to demonstrate that the surface enrichment of Pt in Pt/Ni should occur. Our previous work on Pt/Ru, Pt/Os, and Pt/Ru/Os arc-melted smooth electrodes[16] as well as this work confirms this prediction.

Oxygen *1s* spectra are shown in Figure 9 for Pt/Ni(1:1), Pt/Ni(3:1), and Pt/Ru/Ni(5:4:1). The relative atomic structure composition of the various oxygen species is dependent on the composition of the alloy. Curve fitting of the O*1s* signal gives three different peaks, generally with different binding energies. In Pt/Ni(1:1) and Pt/Ni(3:1), peaks with binding energies of

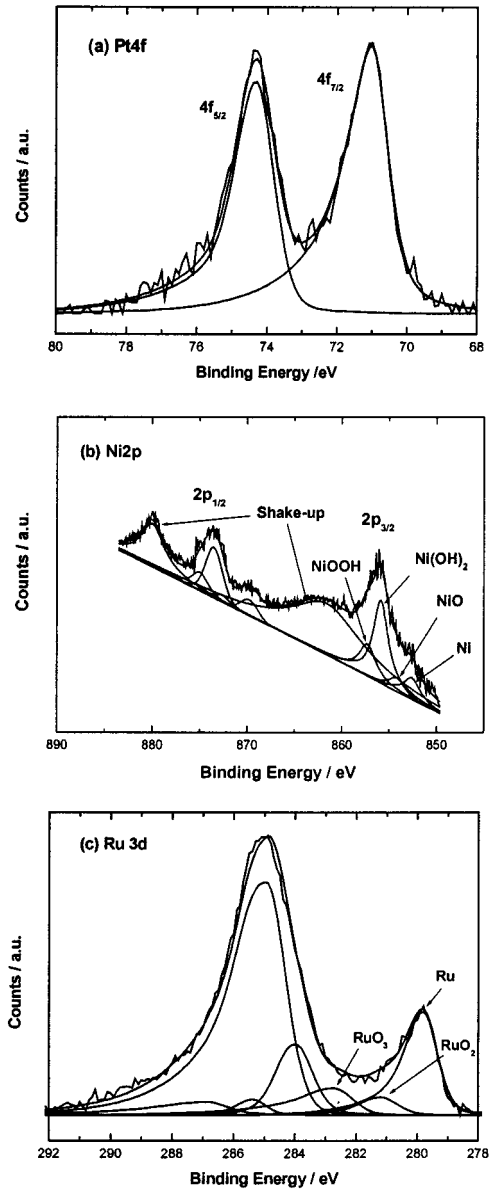


**Figure 7.** X-ray photoelectron spectra of (a) Pt*4f*, (b) Ni*2p*, and (c) Ru*3d* in Pt/Ru/Ni(5:4:1) nanoparticle.

**TABLE 2: Chemical States and Area Ratios of Pt/Ni and Pt/Ru/Ni Alloy Nanoparticles by XPS**

| | XPS area ratio (%) | | |
|---|---|---|---|
| chemical states | Pt/Ni(1:1) | Pt/Ni(3:1) | Pt/Ru/Ni(5:4:1) |
| metallic Ni | 11.8 | 33.7 | 14.4 |
| NiO | 15.9 | 8.8 | 11.2 |
| $Ni(OH)_2$ | 45.2 | 35.7 | 46.3 |
| NiOOH | 27.1 | 21.8 | 28.1 |

529.0, 530.8−531.2, and 532.8−533.1 eV are assigned to $O^{2-}$, $OH^-$, and adsorbed oxygen or hydroscopic (incorporated) water, respectively.[69,70] However, O*1s* in Pt/Ru/Ni(5:4:1) represents three oxygen species in terms of the *1s* signals of $RuO_2/RuO_3$ at 529.8 eV, of $Ru(OH)_x$ at 532.8 eV, and of the adsorbed oxygen form at 533.6 eV. O*1s* of $Ru(OH)_x$ shifts from the literature data of 532.4 eV because of the contribution from Ni hydroxide.[75]

It has recently been reported that nickel or nickel hydroxides acting as a catalyst not as a promoter or supporter are capable of oxidizing methanol in alkaline or acid solution. Kowal et al.[76] and El-Shafei[77] investigated nickel hydroxide (NiOOH/$Ni(OH)_2$) on the nickel metal electrode for methanol oxidation

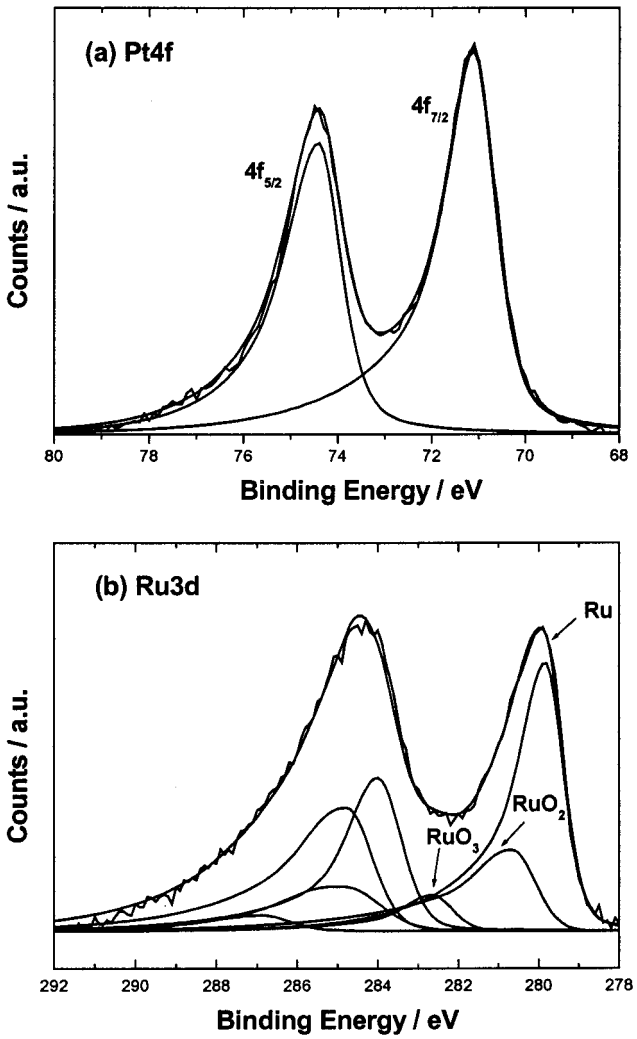


**Figure 8.** X-ray photoelectron spectra of (a) Pt*4f* and (b) Ru*3d* in Pt/Ru(1:1) nanoparticle.

in alkaline solutions (NaOH and KOH). On the other hand, methanol oxidation in acidic solution was performed by Manoharan et al.[78] The authors proposed that methanol oxidation occurred on the oxyhydroxide films of the Ni in Ni/Ti alloy electrode. The following reaction schemes were proposed, noteworthy including nickel hydroxide as the reagent for methanol oxidation:

$$2Ni^{3+}O^{2-} + CH_3OH \leftrightarrow Ni^{2+}OH^- + Ni^{2+}O^-CH_2OH \rightarrow Ni^{3+}O^{2-} + Ni^{3+}O^-C^-HO + 3H^+ + e^-$$

$$Ni^{3+}O^-C^-HO \rightarrow Ni^{3+}O^-C^- = O + H^+ + e^- \rightarrow Ni^{3+}O^{2-} + CO_2 + 2H^+ + 2e^- \quad (3)$$

The reaction is completed with an attack by water on a surface carboxyl group. In addition, according to the reversible redox in reaction scheme 3, $Ni^{II}(OH)_2$ in the $CH_3OH/H_2SO_4$ solution can be converted to $Ni^{III}OOH$, which is a stable phase in the catalyst:[79]

$$Ni(OH)_2 \leftrightarrow NiOOH + H^+ + e^- \quad (4)$$

The surface layer of the Pt/Ni or Pt/Ru/Ni contains both $Ni^{II}(OH)_2$ and $Ni^{III}OOH$ (see above). The mixed-valence $Ni^{3+/2+}$

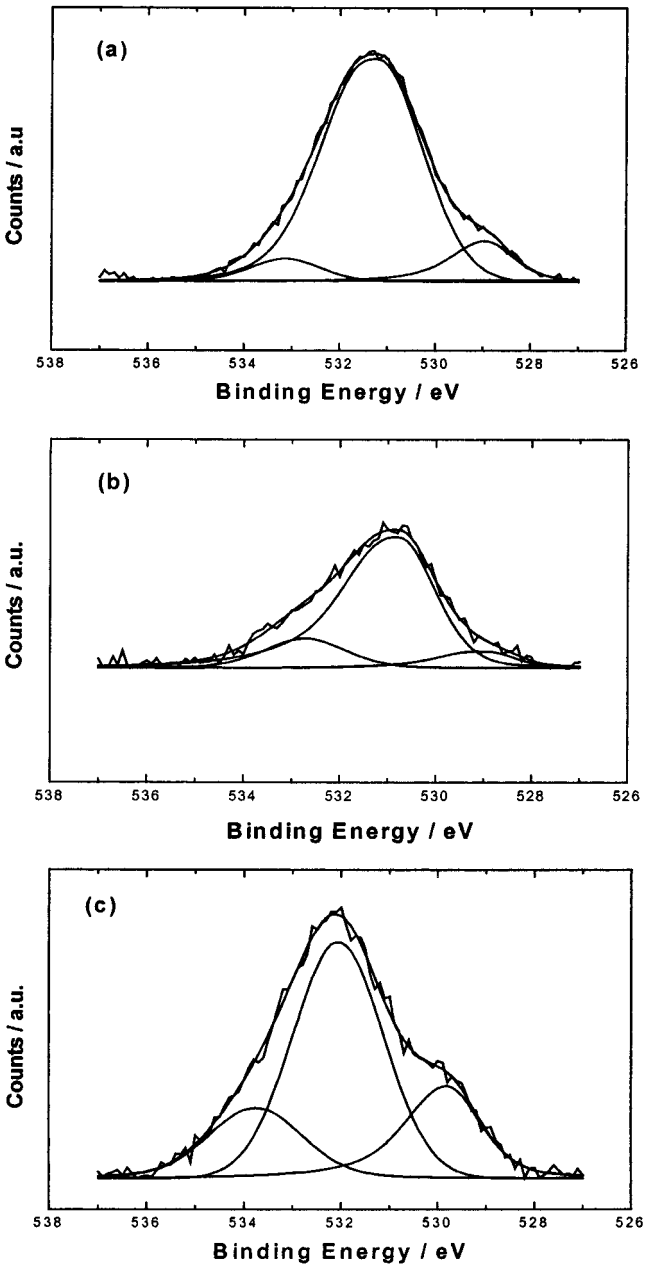


**Figure 9.** X-ray photoelectron spectra of O*1s* in (a) Pt/Ni(1:1), (b) Pt/Ni(3:1), and (c) Pt/Ru/Ni(5:4:1) nanoparticles.

components account for the high electronic conductivity of the surface layer, are relatively stable in acidic media, and have a confirmed catalytic activity.[80] The Ni hydroxide layer has some other favorable properties, such as proton and electronic conductivity, and are well protected from corrosion under methanol oxidation conditions. Such a hydroxide layer on the Pt/Ni and Pt/Ru/Ni may display high catalytic activity with respect to methanol oxidation. Therefore, we propose the following reaction scheme for Pt/Ni nanoparticles:

$$\mathrm{NiOOH} + x\mathrm{Pt{-}H} \rightarrow \mathrm{Ni(OH)_2} + x\mathrm{Pt}$$

$$\mathrm{Ni(OH)_2} \rightarrow \mathrm{NiOOH} + \mathrm{H^+} + \mathrm{e^-} \qquad (5)$$

In contrast to various chemical states of Ni, as seen in Figure 9, Pt in Pt/Ni and Pt/Ru/Ni consist of elemental state of platinum ($Pt^o$), which provides more suitable sites for methanol decomposition than $Pt^{II}O$ or $Pt^{IV}O_2$. Hence, the existence of Pt metal

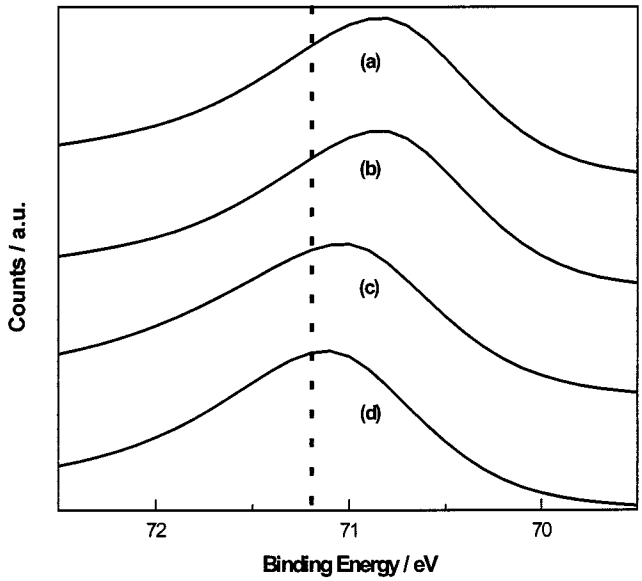


**Figure 10.** Pt*4f* peak shift of Pt-based nanoparticles; (a) Pt/Ni(1:1), (b) Pt/Ni(3:1), (c) Pt/Ru/Ni(5:4:1), and (d) Pt/Ru(1:1). The dotted line is the $Pt4f_{7/2}$ peak position for pure Pt.

**TABLE 3: Pt*4f* Peak Shifts for Pt-Based Alloy Nanoparticles by XPS**

| | Pt*4f* (eV) | |
|---|---|---|
| Pt alloys | $4f_{7/2}$ | $4f_{5/2}$ |
| Pt/Ni (1:1) | 70.85 | 74.15 |
| Pt/Ni (3:1) | 70.84 | 74.14 |
| Pt/Ru/Ni (5:4:1) | 71.03 | 74.33 |
| Pt/Ru (1:1) | 71.11 | 74.41 |
| pure Pt | 71.20 | 74.53 |

on the catalyst is essential for high surface activity with respect to methanol oxidation.

**Electronic Effect in Pt/Ni-Based Electrocatalysts.** The average particle size of the alloy nanoparticles investigated in this paper is less than 4 nm. From the escape depth of about 2−3 nm of photoelectrons for Pt, Ru, and Ni, it is clear that the entire bulk was the subject to the XPS scrutiny. XPS Pt*4f* spectra for Pt/Ni and Pt/Ru/Ni alloy nanoparticles are shown in Figure 10 and Table 3 and are compared to the spectrum obtained from pure Pt (the vertical dotted line in Figure 10). The peaks are shifted from −0.17 for Pt/Ru/Ni(5:4:1) to −0.35 and −0.36 eV at Pt/Ni; that is, they are moving toward the lower Pt*4f* biding energy. Because there is more metallic nickel in Pt/Ni(1:1) than in other Ni-containing formulations studied in this project, the combined XPS and XRD data demonstrate that the spectral shift increases, at least semiquantitatively, with the amount of Ni metal present in the sample, see Figures 1 and 10. Overall, we have collected evidence for the change in the electronic structure of Pt when it was alloyed with nickel (and partially with ruthenium, Figure 10). This change may modify the electrocatalytic activity of platinum in the methanol electrooxidation process. For ruthenium, only a small binding energy change for Pt was observed because of ruthenium addition, but it was better resolved than in our previous investigations of the arc-melted Pt/Ru disk[16] and platinum surfaces decorated by ruthenium.[81]

As to the small Ru shift mentioned above, the literature survey indicates that XPS evidence for the electronic effect in Pt/Ru catalysts is not definite. Goodenough et al.[17] reported a Pt*4f* XPS shift in the Pt/Ru/C samples prepared by the impregnation method, which was considered indicative of the lowering Pt

binding energy (BE) because of the Ru additive, as in this work. It was concluded that electron transfer occurred from Ru to Pt. It was also concluded that the charge-transfer enhanced adsorption of oxygen species from electrolyte to the surface. In the first approximation, the charge transfer from ruthenium to platinum is consistent with lowering the stretching frequency (red shift) in CO on Pt/Ru alloy[16] or in CO chemisorbed on the Pt phase of the Ru decorated Pt electrodes.[51] Recently, however, Toda et al.[18] discussed the electronic properties of Pt-based alloy catalysts involved in an oxygen reduction reaction (in PEMFC). A higher BE shift of Pt in 60 nm sputtered Pt/Ni, Pt/Co, and Pt/Fe films on a Ti/glass substrate was reported. The enhancing mechanism in oxygen reduction was discussed as the consequence of lowering the Fermi level or because of the increased d electron vacancy in the 5d Pt band caused by the underlying alloy. Even more recently, Giorgi et al. have reported a Pt XPS peak shift in Pt/Ru alloy nanoparticles toward higher binding energy.[50]

In this report, we found that there was electron transfer from nickel to platinum in Pt/Ni and Pt/Ru/Ni and, probably, from ruthenium to platinum in Pt/Ru, in agreement with the electronegativity series for Ni, Ru, and Pt: 1.91, 2.2, and 2.28,[51] respectively. The Pt/Ru displays a small XPS shift as compared to Pt/Ni, consistent with the smaller difference in the electronegativity between Ru and Pt versus that between Ni and Pt. The small difference in the electronegativity for Ru and Pt may also explain why XANES data are not conclusive enough as to the relation between higher Pt d vacancies and the electrocatalytic activity.[82] At the same time, we obtained improved electrocatalytic results in Pt/Ni alloys, as seen in CV and CA. One way to interpret it is that the shift of d electron density from Ni to Pt would lower DOS on the Fermi level and reduce the Pt−CO bond energy. Using NMR, we have already found a reduction in $2\pi^*$ DOS of CO on Pt/Ru versus that for pure Pt.[41,83,84] Although the electronic interpretation of the catalytic enhancement results is quite tempting, we also pointed out above that Ni (hydro)oxides on the Pt/Ni and Pt/Ru/Ni nanoparticles could promote methanol oxidation via a surface redox process. The balance between these two contributions to the enhancement will have to be established in further studies.[14]

**Dissolution of Nickel Metal.** It has been reported that, at potentials $E < 0.6$ V, the dissolution of Ni takes place at a Ni electrode in acid solution.[85] However, no dissolution of Ni in the Pt/Ni(1:1) alloy catalyst was observed in the potential range of 0∼1.6 V (NHE) (Figure 11). In the potential range of methanol oxidation, Ni is passive and not very much susceptible to corrosion. Although some dissolution of Ni could take place, the amount of dissolution from the Pt lattice is apparently very small. This indeed implies that in our samples nickel metallic state is either passivated by Ni hydroxides or exists as a stable phase in the platinum lattice. Barnett et al.[86] concluded that carburized NiW displayed not only passivity but also some electrocatalytic activity without Ni dissolution, the behavior that we here confirm. This implies that nickel in the Pt/Ni nanoparticles can be stabilized by the Pt lattice in acidic media. More experiments are underway to evaluate the long-term stability of these materials.

## Conclusions

Electrocatalytic activity of Pt/Ni alloy nanoparticles, formed by reduction with $NaBH_4$ of the inorganic salt precursors and freeze-drying, was investigated with respect to the oxidation of methanol in $H_2SO_4$ solutions. The Pt/Ni based catalysts display catalytic activity superior to that of pure Pt. The onset potential for methanol oxidation is Pt/Ru/Ni(5:4:1) < Pt/Ru(1:1) < Pt/Ni(1:1) ≈ Pt/RuNi(6:3.5:0.5) < Pt/Ni(3:1) < pure Pt. XPS data confirm that Ni and Ru additives to Pt exist as mixed metal/oxide phases, whereas Pt is entirely metallic. In the Pt/Ni alloy nanoparticles, the Ni species include metallic Ni, NiO, $Ni(OH)_2$, and NiOOH, and the ratio between the three oxides is similar for the different Pt/Ni alloys. The binding energy shift for Pt in the Pt/Ni nanoparticles was identified by XPS and is interpreted to result from the modification of electronic structure of platinum by electron transfer from Ni to Pt. We believe that the electron transfer may contribute to the enhanced CO oxidation (CO generated from methanol decomposition), that is, to the CO tolerance on the Ni-containing composites, in comparison to pure Pt samples. However, the competing effect in the Ni enhancement may be due to the surface redox activity of Ni oxides toward the CO. Our results show that the onset potential and the long time current delivery of Pt/Ru/Ni(5:4:1) are superior to that of Pt/Ru(1:1). Currently, this comparison is limited to the catalysts synthesized by the borohydride reduction method combined with freeze-drying and not to commercial catalysts. Further work is needed to evaluate such laboratory catalysts for fuel cell applications. However, this opens the possibility for a systematic approach to design new Ni− containing platinum catalytic nanoparticles, and the corresponding investigations are underway.

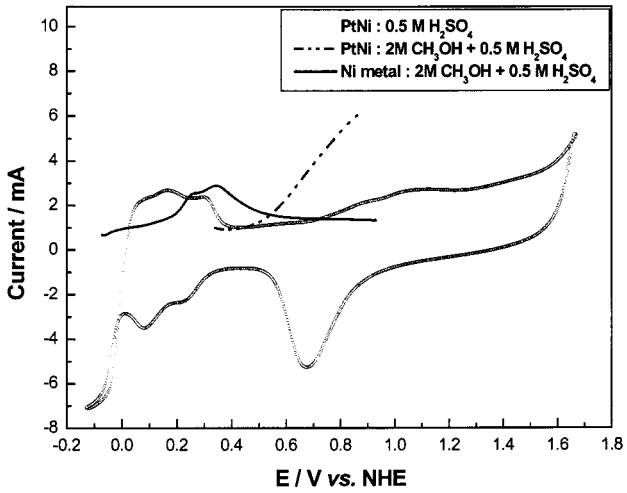


**Figure 11.** Potential−current plots of Ni metal and Pt/Ni(1:1) nanoparticle at the range of methanol oxidation voltage in 2.0 M $CH_3OH$ + 0.5 M $H_2SO_4$ with the scan rate of 50 mV $s^{-1}$ at room temperature.

**Acknowledgment.** This work was supported by the Korea Energy Management Corporation and the Brain Korea 21 Project from the Ministry of Education. A.W. acknowledges support by the United States Department of Energy under the Grant DEFG02-96ER45439, administered by the Frederic Seitz Materials Research Laboratory at UIUC. XPS work was carried out at the Center for Microanalysis of Materials, University of Illinois at Urbana−Champaign, which is supported by the U.S. Department of Energy under Contract No. DEFG02-91-ER45439.

## References and Notes

(1) Hearth, M. P.; Hards, G. A. *Platinum Met. Rev.* **1996**, *40*, 150.
(2) Oetjen, H.-F.; Schmidt, V. M.; Stimming, U.; Trila, F. *J. Electrochem. Soc.* **1996**, *143*, 3838.
(3) Hamnett, A. *Catal. Today* **1997**, *38*, 445.
(4) Reddington, E.; Sapienza, A.; Gurau, B.; Viswanathan, R.; Sarangapani, S.; Smotkin, E. S.; Mallouk, T. E. *Science* **1998**, *280*, 1735.

(5) Ross, P. N. In *Electrocatalysis*; Lipkowski, J., Ross, P. N., Eds.; Wiley-VCH: New York, 1998; Chapter 2.
(6) Wieckowski, A., Ed.; In *Interfacial Electrochemistry*; Marcel-Dekker: New York, 1999; Chapters 44−51.
(7) Chrzanowski, W.; Kim, H.; Wieckowski, A. *Catal. Lett*. **1998**, *50*, 69.
(8) Chrzanowski, W.; Kim, H.; Tremiliosi-Filho, G.; Wieckowski, A.; Grzybowska, B.; Kulesza, P. *J. New. Mater. Electrochem. Syst.* **1998**, *1*, 31.
(9) Chrzanowski, W.; Wieckowski, A. *Langmuir* **1997**, *13*, 5974.
(10) Gasteiger, H. A.; Markovic, N.; Ross, P. N.; Cairns, E. J. *J. Phys. Chem.* **1993**, *97*, 12020.
(11) Gasteiger, H. A.; Markovic, N.; Ross, P. N.; Cairns, E. J. *J. Electrochem. Soc*. **1994**, *141*, 1795.
(12) Gasteiger, H. A.; Markovic, N.; Ross, P. N.; Cairns, E. J. *Electrochim. Acta*. **1994**, *39*, 1825.
(13) Gasteiger, H. A.; Markovic, N.; Ross, P. N.; Cairns, E. J. *J. Phys. Chem.* **1994**, *98*, 617.
(14) Herrero, E.; Franaszczuk, K.; Wiekowski, A. *J. Phys. Chem*. **1994**, *98*, 5074.
(15) Watanabe, M.; Motoo, S. *J. Electroanal. Chem*. **1975**, *60*, 275.
(16) Liu, R.; Iddir, H.; Fan, Q.; Hou, G.; Bo, A.; Ley, K. L.; Smotkin, E. S.; Sung, Y.-E.; Kim, H.; Thomas, S.; Wieckowski, A. *J. Phys. Chem. B.* **2000**, *104*, 3518.
(17) Goodenough, J. B.; Manoharan, R.; Shukla, A. K.; Ramesh, K. V. *Chem. Mater*. **1989**, *1*, 391.
(18) Toda, T.; Igarashi, H.; Uchida, H.; Watanabe, M. *J. Electrochem. Soc*. **1999**, *146*, 3750.
(19) Herrero, E.; Feliu, J. M.; Wieckowski, A. *Langmuir* **1999**, *15*, 4944.
(20) Chrzanowski, W.; Wieckowski, A. *Langmuir* **1998**, *14*, 1967.
(21) Kim, H.; Tremiliosi-Filho, G.; Sung, Y.-E.; Wieckowski, A. In *3rd Int. Sym. Electrocatal*.; Hocevar, S., Gaberscek, M., Pintar, A., Eds.; NIC: Slovenia, 1999; p 213.
(22) Sung, Y.-E.; Thomas, S.; Wieckowski, A. *J. Phys. Chem*. **1995**, *99*, 13513.
(23) Thomas, S.; Sung, Y.-E.; Kim, H. S.; Wieckowski, A. *J. Phys. Chem.* **1996**, *100*, 11726.
(24) Sung, Y.-E.; Chrzanowski, W.; Zolfaghari, A.; Jerkiewicz, G.; Wieckowski, A. *J. Am. Chem. Soc*. **1997**, *119*, 194.
(25) Han, M.; Mrozek, P.; Wieckowski, A. *Phys. Rev. B*. **1993**, *48*, 8329.
(26) Min, M.-K.; Cho, J.; Cho, K.; Kim, H. *Electrochim. Acta* **2000**, *45*, 4211.
(27) Wasmus, S.; Küver, A. *J. Electroanal. Chem*. **1999**, *461*, 14.
(28) Frelink, T.; Visscher, W.; van Veen, J. A. R. *J. Electroanal. Chem*. **1995**, *382*, 65.
(29) Christensen, P. A.; Hamnett, A.; Munk, J.; Troughton, G. L. *J. Electroanal. Chem*. **1994**, *370*, 251.
(30) Watanabe, M.; Saegusa, S.; Stonehart, P. *J. Electroanal. Chem*. **1989**, *271*, 213.
(31) Kennedy, B. J.; Hamnett, A. *J. Electroanal. Chem*. **1990**, *283*, 271.
(32) Burke, L. D.; Casey, J. K. *Ber. Bunsen-Ges. Phys. Chem*. **1990**, *94*, 931.
(33) Mukerjee, S.; McBreen, J. *J. Electroanal. Chem*. **1998**, *448*, 163.
(34) Day, J. B.; Vuissoz, P. A.; Oldfield, E.; Wieckowski, A.; Ansermet, J. P. *J. Am. Chem. Soc.* **1996**, *118*, 13046.
(35) Tong, Y.-Y.; Oldfield, E.; Wieckowski, A. *Anal. Chem*. **1998**, *70*, 518A.
(36) Tong, Y.-Y.; Rice, C.; Wieckowski, A.; Oldfield, E. *J. Am. Chem. Soc.* **2000**, *122*, 1123.
(37) Abraham, F. F.; Tsai, N.-H.; Pound, G. M. *Surf. Sci*. **1979**, *83*, 406.
(38) De Temmerman, L.; Creemers, C.; Van Hove, M.; Neyens, A.; Bertolini, J.; Messardier, J. *Surf. Sci*. **1986**, *178*, 888.
(39) McNicol, B. D.; Short, R. T. *J. Electroanal. Chem*. **1977**, *81*, 249.
(40) Goodman, D. W. *J. Phys. Chem.* **1992**, *96*, 7814.
(41) Tong, Y. Y.; Kim, H. S.; Babu, P. K.; Waszczuk, P.; Wieckowski, A.; Oldfield, E. *J. Am. Chem. Soc*. Submitted for publication.
(42) Rodriguez, J. A.; Goodman, D. W. *Science* **1992**, *257*, 897.
(43) Jinang, X.; Permeter, J. E.; Estrada, C. A.; Goodman, D. W. *Surf. Sci*. **1991**, *249*, 44.
(44) Ishikawa, Y.; Liao, M. S.; Cabrera, C. R. *Surf. Sci*. **2000**, *463*, 66.
(45) Lide, D. R., Ed; In *CRC Handbook of Chemistry & Physics*, 81th ed.; CRC Press: Boca Raton, FL, **2000**; pp 9−51.
(46) Ley, K. L.; Liu, R.; Pu, C.; Fan, Q.; Leyarovska, N.; Segre, C.; Smotkin, E. S. *J. Electrochem. Soc*. **1997**, *144*, 1543.
(47) Gurau, B.; Viswanathan, R.; Liu, R.; Lafrenz, T. J.; Ley, K. L.; Smotkin, E. S.; Reddington, E.; Sapienza, A.; Chan, B. C.; Mallouk, T. E.; Sarangapani, S. *J. Phys. Chem. B* **1998**, *102*, 9997.
(48) Liu, R.; Ley, K. L.; Pu, C.; Fan, Q.; Leyarovska, N.; Segre, C.; Smotkin, E. S. In *Electrode Processes VI*; Wieckowski, A., Itaya, K., Eds.; The Electrochemical Society: Pennington, NJ, 1996; p 341.
(49) McBreen, J.; Mukerjee, S. *J. Electrochem. Soc*. **1995**, *142*, 3399.
(50) Giorgi, L.; Pozio, A.; Bracchini, C.; Giorgi, R.; Turtu, S. *J. Appl. Electrochem.* **2001**, *31*, 325.
(51) Friedrich, K. A.; Geyzers, K.-P.; Linke, U.; Stimming, U.; Stumper, J. *J. Electroanal. Chem.* **1996**, *402*, 123.
(52) Kinoshita, K.; Stonehart, P. *Modern Aspect of Electrochemisty*, Plenum Press: New York, 1996; p 12.
(53) Klabunde, K. J.; Mohs, C. In *Chemistry of Advance Materials*; Interrante, L. V., Hampden-Smith, L. V., Eds.; Wiley-VCH: New York, 1998; Chapter 3.
(54) Shirley, D. A. *Phys. Rev. B* **1972**, *5*, 4709.
(55) Sherwood, P. M. A. In *Practical Surface Analysis*; Briggs, D., Seah, M. P., Ed.; Wiley: New York, 1990; Appendix 3.
(56) Moulder, J. F.; Stickle, W. F.; Sobol, P. E.; Bomben, K. D. *Handbook of X-ray Photoelectron Spectroscopy*; Chastin, J., Ed.; Physical Electronics: Eden Prairie, MN, 1992.
(57) Wagner, C. D.; Davis, L. E.; Zeller, M. V.; Taylor, J. A.; Raymond, R. M.; Gale, L. H. *Surf. Interface Anal*. **1981**, *3*, 211.
(58) Chan, R. W. M.; Kwok, R. W. M.; Lau, W. M.; Yan, H.; Wong, S. P. *J. Vac. Sci. Technol. A* **1997**, *15*, 2787.
(59) Wilson, M. S.; Gottesfeld, S. *J. Appl. Electrochem*. **1992**, *22*, 1.
(60) Radmilovic, V.; Gasteiger, H. A.; Ross, P. N., Jr. *J. Catal.* **1995**, *154*, 98.
(61) Kim, K. S.; Winograd, N. *Surf. Sci*. **1974**, *43*, 623.
(62) McIntyre, N. S.; Cook, M. G. *Anal. Chem*. **1975**, *47*, 2208.
(63) Mitton, D. B.; Walton, J.; Thomson, G. E. *Surf. Interface Anal*. **1993**, *20*, 36.
(64) Shulz, R.; Van Neste, A.; Zielinski, P. A.; Boily, S.; Czerwinski, F.; Szpunar, J.; Kaliaguine, S. *Catal. Lett.* **1995**, *35*, 89.
(65) Hoppe, H.-W.; Strehblow, H.-H. *Surf. Interface Anal*. **1989**, *14*, 121.
(66) Klein, J. C.; Hercules, D. M. *J. Catal*. **1983**, *82*, 424.
(67) Ng, K. T.; Hercules, D. M. *J. Phys. Chem*. **1976**, *80*, 2094.
(68) Paul, D. K.; Xie, Y.; Sherwood, P. M. A. *Anal. Chem.* **1993**, *65*, 2276.
(69) Luo, P. F.; Kuwana, T.; Paul, D. K.; Sherwood, P. M. A. *Anal. Chem*. **1996**, *68*, 3330.
(70) Casella, I. G.; Guascito, M. R.; Sannazzaro, M. G. *J. Electroanal. Chem*. **1999**, *462*, 202.
(71) Jeong, D.-J.; Kim, W.-S.; Sung, Y.-E. *Jpn. J. Appl. Phys.* **2001**, *40*, L708.
(72) Jeong, D.-J.; Kim, W.-S.; Choi, Y.-K.; Sung, Y.-E. *J. Electroanal. Chem.* **2001**, *511*, 79.
(73) Lide, D. R., Ed. *CRC Handbook of Thermophysical and Thermochemical Data*, CRC Press: Boca Raton, FL; 1994.
(74) Mukherjee, S.; Moran-Lopez, J. L. *Surf. Sci*. **1987**, *189−190*, 1135.
(75) Vukovic, M.; Valla, T.; Milun, M. *J. Electroanal. Chem*. **1993**, *356*, 81.
(76) Kowal, A.; Port, S. N.; Nichols, R. J. *Catal. Today*. **1997**, *38*, 483.
(77) El-Shafei, A. A. *J. Electroanal. Chem*. **1999**, *471*, 89.
(78) Manoharan, R.; Goodenough, J. B. *J. Mater. Chem*. **1992**, *2*, 875.
(79) Bode, H.; Dehmelt, K.; Witte, J. *Electrochim. Acta*. **1996**, *11*, 1097.
(80) Horkans, J.; Shafer, M. W. *J. Electrochem. Soc*. **1977**, *124*, 1196.
(81) Kim, H.; Rabelo de Moraes, I.; Tremiliosi-Filho, G.; Haasch, R.; Wieckowski, A. *Surf. Sci.* **2001**, *474*, L203.
(82) Mukerjee, S.; Srinivasan, S.; Soriaga, M. P.; McBreen, J. *J. Phys. Chem.* **1995**, *99*, 4577.
(83) Hammer, B.; Morikawa, Y.; Norskov, J. K. *Phys. Rev. Lett*. **1996**, *76*, 2141.
(84) Ruban, A.; Hammer, B.; Stoltze, P.; Skriver, H. L.; Norskov, J. K. *J. Mol. Catal. A: Chem*. **1997**, *115*, 421.
(85) Arvia, A. J.; Posadas, D. In *Encyclopedia and electrochemistry of the Elements*; Bard, A. J., Ed.; M. Dekker: New York, 1975; p 3.
(86) Barnett, C. J.; Burstein, G. T.; Kucernak, A. R. J.; Williams, K. R. *Electrochim. Acta*. **1997**, *42*, 2381.